Virus assembly

DOI: 10.1002/smll.200600399

Rapid Deposition and Long-Range Alignment of Nanocoatings and Arrays of Electrically Conductive Wires from Tobacco Mosaic Virus**

Daniel M. Kuncicky, Rajesh R. Naik, and Orlin D. Velev**

Nanostructured and mesoscopically ordered architectures based on biomaterial templates may be used in making integrated mechanical, optical, and electronic devices.[1] A scheme for fabricating such devices will likely employ patterned functional biomaterials, which are used as scaffolds for the directed growth of inorganic materials. Tobacco mosaic virus (TMV) and M13 bacteriophage are particularly interesting as bioscaffolds owing to the combined chemical functionality of the virus protein coat, low size polydispersity, liquid-crystalline organization, and length scales that bridge the gap between traditional bottom-up and top-down fabrication schemes.[2] Recent advances in the biomimetic synthesis of inorganic materials by using genetically engineered viruses and proteins have opened the door to new organic–inorganic composites containing metals, silica, and semiconductors.[3–10] The major challenge in using such bioscaffolds in technology lies in developing new surface-patterning techniques that are controllable, reproducible, and efficient.

We report here a versatile technique for rapidly assembling large-scale nanocoatings and ordered fibers from tobacco mosaic virus and converting them into electrically functional structures. The nanofilms were deposited by pulling, with a constant rate, a meniscus containing the virus suspension. Current molecular and colloidal self-assembly techniques for patterning surfaces with functional biomaterials include Langmuir–Blodgett lithography,[11–13] templating in sessile droplets with imposed shear,[14–18] self-assembly driven by dewetting or chemoselective interactions on micropatterned surfaces,[19–22] and electrostatic layer-by-layer assembly.[23] The technique that we report here uses an alternative flow assembly technique for organizing and aligning TMV into fibers and wires on surfaces. These films were of controlled thickness, structure, and long-range virus orientation, properties achieved by a combination of shear and dewetting. The density and branching of the virus wires were controlled by varying the substrate wettability and the meniscus withdrawal speed. The virus fibers were converted into anisotropically conductive arrays of wires of lengths of multiple centimeters by conjugation of gold nanoparticles followed by silver-metal deposition.

TMV is a rod-shaped virus (300 nm in length and 18 nm in diameter), which forms lyotropic liquid crystals. Above a certain critical concentration, suspensions of TMV undergo an isotropic–nematic (I–N) transition.[24] Although the suspensions used here are well below the concentration required for the I–N transition, the formation of phase-separated aggregates can be observed in drying droplets. When droplets of this TMV suspension on a surface were allowed to evaporate, they exhibited alignment of linear virus aggregates normal to the three-phase contact line (Figure 1b). As the meniscus receded, these aggregates were deposited as fibers and strands onto the substrate. Although deposition from sessile drops may be useful for fabricating multiplexed arrays of TMV dots and patches, we want to be able to exert operational control over the fiber orientation for the long-range alignment of nanocoatings and wires. This could be achieved by pulling a meniscus containing the virus suspension over a substrate by using an apparatus for controlled colloidal deposition similar to the one developed by us for convective nanoparticle assembly (shown schematically in Figure 1a).[25] However, in contrast to the results of our earlier studies on particle crystallization with this experimental setup,[26] the evaporation at the air–liquid interface near the three-phase contact line (leading to convective assembly) was found to have a minimal effect on the assembly of the TMV into strands and fibers. The organization of TMV in the experiment could be explained by shear-induced virus alignment working in conjunction with dewetting-driven assembly at the three-phase contact line.

We characterized the dependence of the TMV fiber size, packing density, and alignment on how well the aqueous suspension wetted the substrate. Dense arrays of narrow fibers were deposited when a hydrophilic glass substrate (contact angle $<4^\circ$) was used (Figure 1d,e). The diameter of the strands at low concentration (5 mg mL^{-1}, Figure 1d) was typically between four and eight viruses. Deposition of fibers at a higher concentration (40 mg mL^{-1}, Figure 1e) effectively increased the fiber diameter and at the same time decreased the spacing between individual fibers. The parallel linear fibers in both cases were contiguous and span the entire length of the substrate. Coatings with a contiguous structure over lengths of 2–4 centimeters were fabricated. On hydrophilic substrates, atomic force microscopy (AFM)

[*] D. M. Kuncicky, Prof. O. D. Velev
Department of Chemical and Biomolecular Engineering
North Carolina State University
Raleigh, NC 27695 (USA)
Fax: (+1) 919-515-3465
E-mail: odvelev@unity.ncsu.edu
Dr. R. R. Naik
Materials and Manufacturing Directorate
Air Force Research Laboratory, Wright-Patterson AFB
Dayton, OH 45433 (USA)
Fax: (+1) 937-255-1128
E-mail: Rajesh.Naik@WPAFB.AF.MIL

[**] This study was financially supported by the Air Force Office of Scientific Research and DARPA. We gratefully acknowledge the support of the Materials and Manufacturing Directorate in the form of a summer internship (D.M.K.). We thank Dr. Matthew Francis for providing tobacco mosaic virus and Laura A. Sowards for assistance with atomic force microscopy imaging, as well as Dr. David M. Phillips and Dr. Joe M. Slocik for useful discussions.

Supporting information for this article is available on the WWW under http://www.small-journal.com or from the author.

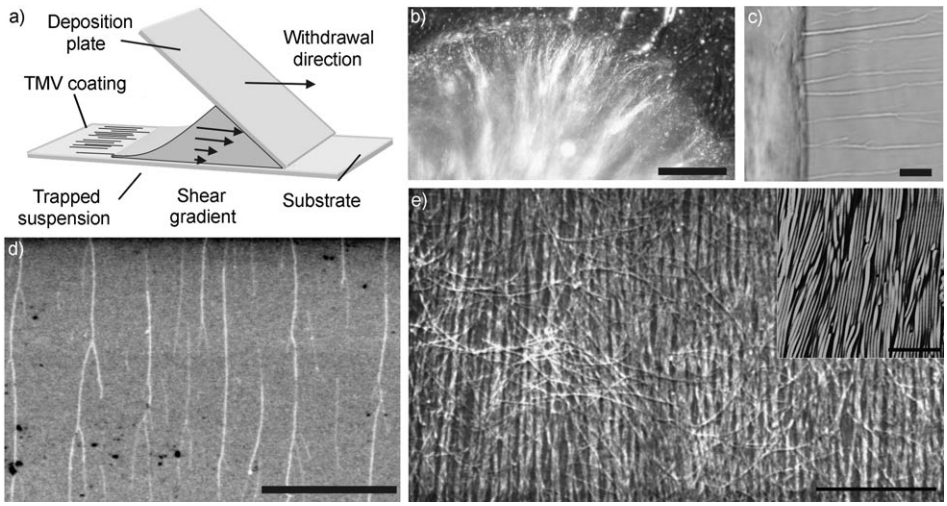

Figure 1. a) Schematic representation of the apparatus for depositing aligned virus-fiber coatings. Typically, virus suspension (20 μL) was entrained between two glass plates held at a fixed angle. The entrained meniscus was dragged across the substrate, and aligned fibers were deposited across the entire surface of the 2.5 × 7.5-cm^2 substrate. b) Bright-field image of a freely receding meniscus showing shear-induced alignment in suspension near the three-phase contact line. c) Phase-contrast optical image of the receding contact line showing TMV-fiber formation on a hydrophobic substrate. Scanning electron microscopy (SEM) image of d) 5 mg mL^{-1} and e) 40 mg mL^{-1} TMV deposited on hydrophilic substrates. Inset: Tapping-mode AFM image of an individual fiber from (e). The scale bars in (b–e) are 500, 100, 5, and 5 μm, respectively, and the scale bar for the inset represents 250 nm.

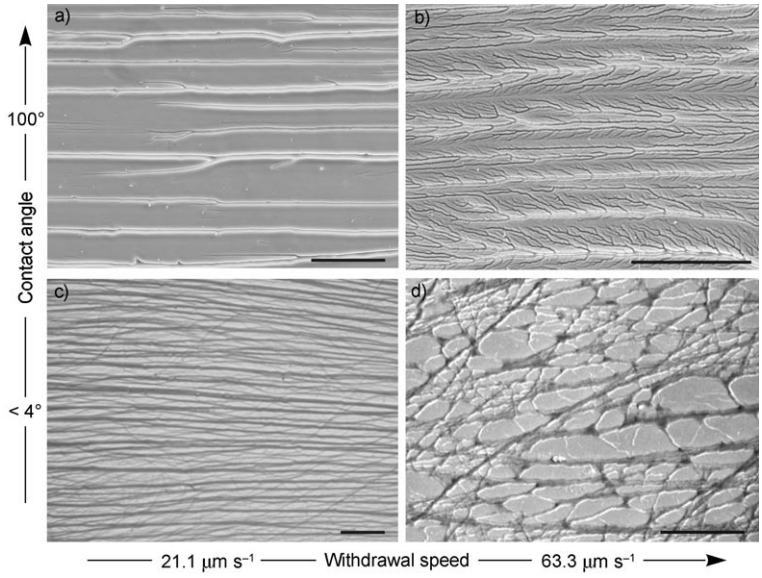

Figure 2. a)–c) Phase-contrast optical and d) SEM images of dried films from TMV fibers showing the effect of substrate wettability and meniscus withdrawal speed on the fiber formation. The scale bars in (a) and (b) are 100 μm and in (c) and (d) are 20 μm.

analysis showed that the individual fibers ranged between 22–85 nm in height (see the Supporting Information), which indicates that the fibers were composed of TMV bundles. However, when a hydrophobized glass surface with advancing contact angle of approximately 100° was used as the substrate, the fibers were thicker, with a width in the order of one micrometer, more branched, and spaced further apart. This indicated that the hydrophobicity of the substrate was a major controlling parameter. Direct observation of the receding meniscus of droplets on such substrates showed that the TMV is deposited by bundling into large fibers at the three-phase contact line (Figure 1c). The fingering at the contact line occurs because of dewetting and breaking of the film on the hydrophobized plate. The fiber-deposition mechanism in the entrained meniscus with imposed shear in the apparatus is probably similar to the one in the sessile droplets, although the meniscus in the apparatus could not be studied by microscopy because it was obscured by the deposition plate.

We investigated systematically the correlation between substrate wettability and meniscus withdrawal speed on the structure of the virus nanocoatings (Figure 2). The results demonstrate that the receding meniscus orients the virus aggregates in solution and that the hydrophobic surfaces invoke further organization of the fibers into contiguous wires by dewetting. TMV suspensions diluted to 40 mg mL^{-1} were used for this part of the investigation. With the exception of experiments at high withdrawal speed (63.3 μm s^{-1}) on the hydrophilic substrate, the fibers were aligned parallel to the direction of meniscus withdrawal, that is, normal to the three-phase contact line. The individual virions were hierarchically organized in the direction of fiber orientation (inset in Figure 1e). This is not surprising since it is known that shear gradients stemming from pressure-induced flow over surfaces or in channels can align anisotropic particles.[27] On the other hand, a surprising result was observed for experiments with high withdrawal speeds on the hydrophilic substrate (Figure 2d). While it was expected that higher withdrawal speeds will produce greater shear forces and even better orientation, the coatings showed a nonaligned weblike morphology. Although the complex interplay of dewetting and shear is not completely understood at this point, our work-

ing hypothesis is that the higher withdrawal speed effectively spreads a thin film onto the substrate before fingering instabilities nucleate fiber growth. Fiber orientation here is random and web-like since the nucleation centers where dewetting begins are not necessarily on the three-phase contact line as seen with slower withdrawal speeds or a freely receding meniscus (Figure 1c).

The structured films deposited on hydrophobized glass substrates, on the other hand, were much better organized in slightly branched parallel fibers (Figure 2a,b; Figure 4a–c). Most of the fibers formed had a core that extended uninterrupted across the entire length of the substrate. High withdrawal speeds promoted formation of thin, highly branched fibers with an average core diameter of approximately 1.5 μm (Figure 2b). Thicker, less-branched fibers with an average diameter of approximately 6 μm (Figure 2a) were formed at the lower withdrawal speed. Fingering instabilities and dewetting-driven assembly have been observed with nanoparticle systems where dewetting occurs at a moving three-phase contact line,[13,28,29] but to our knowledge no one has achieved 2D virus organization on a length scale of multiple centimeters. In summary, the major advantages derived from using this technique are 1) the direction and speed of meniscus withdrawal, and hence the positioning and alignment of fiber deposition, are easily controlled, 2) the method is very efficient, so only microliters of virus suspension are required to coat a standard 2.5×7.5-cm^2 glass microscope slide with parallel fibers of TMV, and 3) the device can be easily scaled up, so the process can be used to coat much larger substrates.

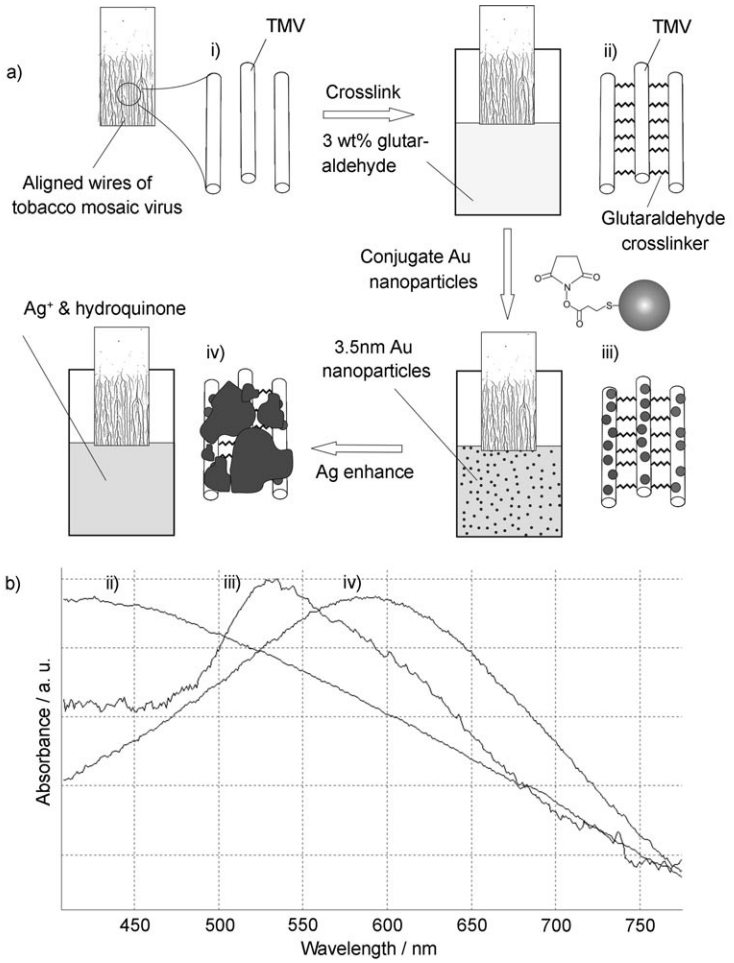

Figure 3. a) Schematic representation of the procedure for fixation, Au nanoparticle conjugation, and Ag enhancement of the TMV wires. b) UV/Vis absorption spectra of the coated substrate after the stages of ii) glutaraldehyde fixation, iii) Au conjugation, and iv) Ag enhancement.

The virus fibers deposited on partially hydrophobized substrates could be used as templates and scaffolds for the fabrication of complex materials with anisotropic electrical conductivity. We demonstrated that these organized virus coatings can be converted into arrays of parallel conducting microwires. A three-step procedure for metallizing the TMV fibers was developed (Figure 3): 1) The fibers were fixed by submerging the coated substrate into a glutaraldehyde solution (3 wt%) for 15 min. The glutaraldehyde cross-linked the TMV virions in the fibers, which also served to prevent the fibers from peeling away during the subsequent metallization step. 2) Gold nanoparticles were attached to the virus surfaces in the fibers. The 10-nm nanoparticles were synthesized by using a citrate reduction protocol and chemically modified with dithiobis(*N*-succinimidyl propionate). The substrates with the fixed virus wires were submerged into the Au particle suspension for two to three hours. The modified Au particles conjugated through the formation of amide bonds to the protein coat on the TMV, although electrostatic effects may also contribute to the binding. Since both the glutaraldehyde fixative from step 1 and the active succinimide ester conjugate from step 2 compete to react with the amines, we found it critical to limit the reaction time with glutaraldehyde such that amine groups on the virus coat remained for attaching Au particles. 3) A silver enhancer kit was used for electroless deposition of a layer of Ag over the conjugated Au particles. All steps in this procedure were followed by extensive washing to remove residual reactants and electrolytes from the surface. We found that a combination of optical microscopy and UV/Vis spectroscopy allowed efficient evaluation of the result of each phase in this process (Figure 3b). A distinct

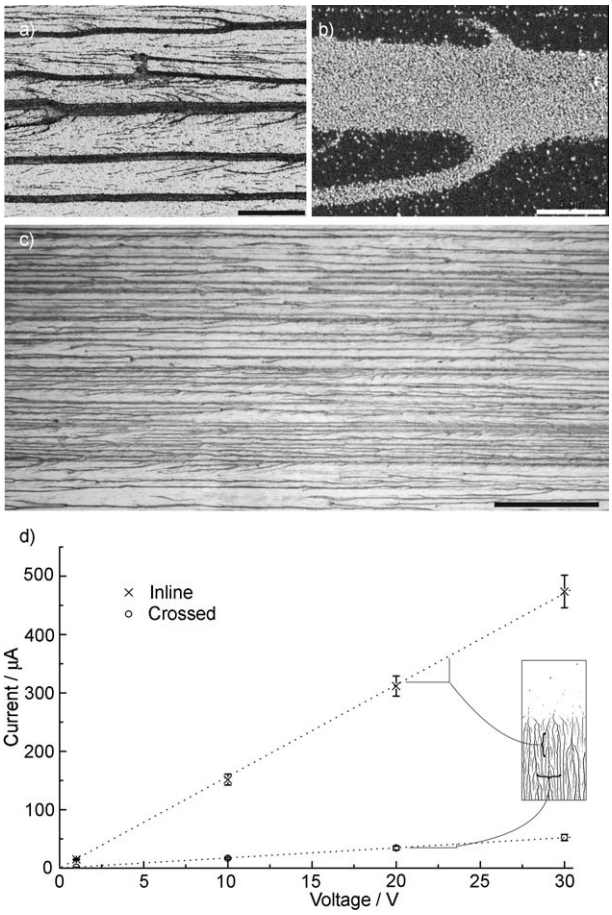

Figure 4. a) and c) Bright-field optical and b) SEM images of metallized virus wires. d) Current–voltage (*I–V*) data for the inline and crossed measurements demonstrating the strong anisotropic conductivity of the virus-wire-coated substrates. Data points are the statistically averaged results from *I–V* sweeps taken on 30 randomly chosen spots over the coated substrate. The scale bars in (a–c) are 50, 5, and 500 μm, respectively.

peak emerged at 530 nm after nanoparticle conjugation due to the Au surface-plasmon absorption bands. This peak widened and red-shifted during Ag enhancement due to the increase in the size of the metal domains. A final peak centering at around 580 nm indicated that the Ag particles were aggregated, at which stage they yielded conductive wires.

The fiber metallization process resulted in substrates coated with arrays of electrically conductive wires spanning areas larger than a few centimeters (Figure 4a–c). The metal-plated virus wires had a difference of one order of magnitude in the values of conductivity between two-terminal measurements inline (parallel) with fiber alignment and measurements orthogonal with fiber alignment. The *I–V* dependence was highly linear ($r^2 = 0.9999$), which shows that the conductivity behavior is ohmic (Figure 4d). The average inline and orthogonal conductivities of a typical substrate measured from the slope of the *I–V* line were 15.7 and 1.7 Ω^{-1}, respectively, thereby proving that the coating is predominantly conductive in the direction of the metallized virus fibers. Direct comparison of these conductivity data to bulk-metal conductivity is problematic owing to the difficulty of accurately estimating the cross-sectional area of the metallized portion of the virus wires. One intriguing question regards the origin of conductivity measured in the direction orthogonal with wire orientation. Based on the microscopy images of the metallized wires (Figure 4a–c), we believe that this conductivity stemmed from nonspecific metallization and occasional overlap between the filamentous branches off the side of the microwires. These two factors are possibly the reason for the low leakage current perpendicular to the direction of alignment of the main wires. The order of magnitude difference in conductivity can possibly be enhanced with further refinement of the metallization and deposition techniques.

In conclusion, we have demonstrated a single-step technique for depositing hierarchically ordered and aligned arrays of virus fibers over macroscopic length scales. The deposition process allows for facile control of the fiber structure through the operational parameters of withdrawal speed and substrate wettability. Shear-induced alignment is largely responsible for the long-range organization during the coating process with these viscous TMV suspensions. By control of the deposition parameters, a range of fiber architectures from linear wires with minimal branching to web-like assemblies were fabricated. A second important process stems from dewetting at the three-phase contact line upon meniscus withdrawal. This results in the deposition of very long contiguous virus fibers. Since the dewetting and shear-induced alignment processes are localized near the three-phase contact line, the process of deposition is size-independent of the volume of entrained liquid. Thereby, the process could be scalable far beyond the centimeter length scales demonstrated here and is only limited by the sizes of the substrate and the deposition apparatus. A procedure was formulated for selectively metallizing these fibers into wires. This allowed the formation of large uniform coatings with highly anisotropic conductivity. Such precisely deposited bioscaffold materials and patterns can find applications in sensors and nanoelectronic, plasmonic, and bioelectronic circuits and devices.

Experimental Section

Materials: Aqueous suspensions of gold nanoparticles were synthesized by using a standard citrate reduction protocol described in the literature.[30] TMV was provided by Dr. Matthew Francis (University of California, Berkeley) and suspended in 10 mM phosphate buffer at pH 6.8. The TMV coatings were deposited onto standard 25 × 75-mm glass microscope slides (Fisher Scientific). Glutaraldehyde (Sigma–Aldrich) for fixation was purchased at 70 wt% and diluted to 3 wt%. Dithiobis(*N*-succinimidyl propionate) (Sigma–Aldrich) powder was dissolved in deionized water to yield a saturated solution before use. An SE-100 silver enhancer kit (Sigma–Aldrich) was used according to the manufacturer's protocol.

Substrate preparation: Prior to virus-wire deposition, glass microscope slides were cleaned in NoChromix (Godax Laboratories) for 12 h, thoroughly washed in deionized water by using a

Millipore RiOs 16 system, and oven dried at 70 °C. This procedure yielded hydrophilic substrates with a water contact angle- $<4^{\circ}$. The hydrophobic substrates with an advancing water contact angle of approximately 100° were prepared by exposing the cleaned glass slides to the vapors of a 1:1 mixture of chlorodimethylsilane (Sigma–Aldrich) and dichlorodimethylsilane (Fluka).

Characterization: Optical micrographs were acquired with an Olympus BX61 optical microscope equipped with a Toshiba PDR-M81 digital camera. SEM imaging of the coated substrates was performed with a JEOL F64 FESEM or a Phillips XL series SEM apparatus at 5–10 kV accelerating voltage. UV/Vis spectroscopy was performed with a Jasco V550 UV/Vis spectrophotometer. AFM data were acquired on a Nanoscope IIIa AFM instrument, under conditions of 1×1-μm^2 phase contrast and a *z*-range phase of 35°. Conductivity measurements were performed by using a two-terminal probe with a 20-mm gap.

General methodology: To verify that the coatings and wires were solely derived from virus deposition and virus-directed bioconjugation for particle assembly, null experiments were performed with solutions containing only buffer. For the null experiments, none of the aforementioned structures were observed.

Keywords:
fibers · microwires · nanocoatings · templates · viruses

[1] C. M. Niemeyer, *Angew. Chem.* **2001**, *113*, 4254; *Angew. Chem. Int. Ed.* **2001**, *40*, 4128.
[2] C. E. Flynn, S. W. Lee, B. R. Peelle, A. M. Belcher, *Acta Mater.* **2003**, *51*, 5867.
[3] W. Shenton, T. Douglas, M. Young, G. Stubbs, S. Mann, *Adv. Mater.* **1999**, *11*, 253.
[4] E. Dujardin, C. Peet, G. Stubbs, J. N. Culver, S. Mann, *Nano Lett.* **2003**, *3*, 413.
[5] S. W. Lee, C. B. Mao, C. E. Flynn, A. M. Belcher, *Science* **2002**, *296*, 892.
[6] T. L. Schlick, Z. B. Ding, E. W. Kovacs, M. B. Francis, *J. Am. Chem. Soc.* **2005**, *127*, 3718.
[7] M. Knez, A. M. Bittner, F. Boes, C. Wege, H. Jeske, E. Maiss, K. Kern, *Nano Lett.* **2003**, *3*, 1079.
[8] J. M. Slocik, R. R. Naik, *Small* **2005**, *1*, 1048.
[9] R. R. Naik, S. E. Jones, C. J. Murray, J. C. McAuliffe, R. A. Vaia, M. O. Stone, *Adv. Funct. Mater.* **2004**, *14*, 25.
[10] D. D. Glawe, F. Rodriguez, M. O. Stone, R. R. Naik, *Langmuir* **2005**, *21*, 717.
[11] X. Michalet, R. Ekong, F. Fougerousse, S. Rousseaux, C. Schurra, N. Hornigold, M. van Slegtenhorst, J. Wolfe, S. Povey, J. S. Beckmann, A. Bensimon, *Science* **1997**, *277*, 1518.
[12] P. Moraille, A. Badia, *Angew. Chem.* **2002**, *114*, 4479; *Angew. Chem. Int. Ed.* **2002**, *41*, 4303.
[13] O. Purrucker, A. Fortig, K. Ludtke, R. Jordan, M. Tanaka, *J. Am. Chem. Soc.* **2005**, *127*, 1258.
[14] T. Heim, S. Preuss, B. Gerstmayer, A. Bosio, R. Blossey, *J. Phys.: Condens. Matter* **2005**, *17*, S703.
[15] J. Raez, J. G. Moralez, H. Fenniri, *J. Am. Chem. Soc.* **2004**, *126*, 16 298.
[16] H. Maeda, *Langmuir* **1999**, *15*, 8505.
[17] Z. X. Deng, C. D. Mao, *Nano Lett.* **2003**, *3*, 1545.
[18] H. Nakao, M. Gad, S. Sugiyama, K. Otobe, T. Ohtani, *J. Am. Chem. Soc.* **2003**, *125*, 7162.
[19] S. R. Whaley, D. S. English, E. L. Hu, P. F. Barbara, A. M. Belcher, *Nature* **2000**, *405*, 665.
[20] H. M. Yi, S. Nisar, S.Y. Lee, M. A. Powers, W. E. Bentley, G. F. Payne, R. Ghodssi, G. W. Rubloff, M. T. Harris, J. N. Culver, *Nano Lett.* **2005**, *5*, 1931.
[21] M. Gleiche, L. F. Chi, H. Fuchs, *Nature* **2000**, *403*, 173.
[22] R. A. Vega, D. Maspoch, K. Salaita, C. A. Mirkin, *Angew. Chem.* **2005**, *117*, 6167; *Angew. Chem. Int. Ed.* **2005**, *44*, 6013.
[23] P. J. Yoo, K. T. Nam, J. F. Qi, S. K. Lee, J. Park, A. M. Belcher, P. T. Hammond, *Nat. Mater.* **2006**, *5*, 234.
[24] S. Fraden, G. Maret, D. L. D. Caspar, R. B. Meyer, *Phys. Rev. Lett.* **1989**, *63*, 2068.
[25] P. Tessier, O. D. Velev, A. T. Kalambur, A. M. Lenhoff, J. F. Rabolt, E. W. Kaler, *Adv. Mater.* **2001**, *13*, 396.
[26] B. G. Prevo, O. D. Velev, *Langmuir* **2004**, *20*, 2099.
[27] Y. Huang, X. F. Duan, Q. Q. Wei, C. M. Lieber, *Science* **2001**, *291*, 630.
[28] A. M. Cazabat, F. Heslot, S. M. Troian, P. Carles, *Nature* **1990**, *346*, 824.
[29] J. X. Huang, F. Kim, A. R. Tao, S. Connor, P. D. Yang, *Nat. Mater.* **2005**, *4*, 896.
[30] J. W. Slot, H. J. Geuze, *Eur. J. Cell Biol.* **1985**, *38*, 87.

Received: August 4, 2006

